Chemical Science

ROYAL SOCIETY OF CHEMISTRY

EDGE ARTICLE

View Article Online
View Journal | View Issue

Cite this: *Chem. Sci.*, 2023, **14**, 7221

All publication charges for this article have been paid for by the Royal Society of Chemistry

Received 15th February 2023
Accepted 3rd June 2023

DOI: 10.1039/d3sc00849e

rsc.li/chemical-science

Evidence for and evaluation of fluorine–tellurium chalcogen bonding†

Robin Weiss,[a] Emmanuel Aubert,[b] Loic Groslambert,[a] Patrick Pale *[a] and Victor Mamane *[a]

In the field of noncovalent interactions, chalcogen bonding (ChB) involving the tellurium atom is currently attracting much attention in supramolecular chemistry and in catalysis. However, as a prerequisite for its application, the ChB should be studied in solution to assess its formation and, if possible, to evaluate its strength. In this context, new tellurium derivatives bearing CH_2F and CF_3 groups were designed to exhibit Te···F ChB and were synthesized in good to high yields. In both types of compounds, Te···F interactions were characterized in solution by combining ^{19}F, ^{125}Te and HOESY NMR techniques. These Te···F ChBs were shown to contribute to the overall J_{Te-F} coupling constants (94–170 Hz) measured in the CH_2F- and CF_3-based tellurium derivatives. Finally, a variable temperature NMR study allowed us to approximate the energy of the Te···F ChB, from 3 kJ mol^{-1} for the compounds with weak Te σ-holes to 11 kJ mol^{-1} for Te σ-holes activated by the presence of strong electron withdrawing substituents.

Introduction

Noncovalent interactions involving halogens and more recently chalcogen atoms are increasingly of interest, especially in materials, crystal engineering, biology, in controlling molecular assembly and more recently in catalysis.[1–4] Highly directional attractive interactions indeed occur between an electron-rich atom (Lewis base) and an electropositive region (σ-hole; Fig. 1)[5] located at the outermost end of a σ-bond involving a halogen or chalcogen atom. In analogy with hydrogen bonds, these interactions were named halogen or chalcogen bonds (XBs or ChBs, respectively).[2,6]

It is now recognized that XBs, especially those involving an iodine atom, also play a key role in biology.[3a,7] Furthermore, ChBs involving sulfur or selenium are now more frequently identified in biostructural and biochemical aspects.[8] A few tellurium compounds have also found biological applications,[9] but so far with no evidence of ChB involvement. On the other hand, fluorine, the most electronegative element, significantly affects the acidity or basicity, bioavailability, lipophilicity, metabolic stability and toxicity of compounds bearing it.[10] Thus, fluorinated compounds increasingly impact pharma- and agro-industries. For example, 28% of newly approved drugs in the last decade (2011–2020) are fluorinated.[10] With its high electronegativity, fluorine is an hydrogen bond (HB) acceptor,[11] but not an XB donor unlike other halogens.[12] Thus, combining both tellurium and fluorine seems worth investigating.[13] However, noncovalent interactions involving fluorine as the acceptor in a ChB remains almost unknown,[14] especially the Te···F interaction.

The extent of a σ-hole on an atom increases with its polarizability and decreases with its electronegativity (Fig. 1).[15] Therefore, iodine is the most effective XB donor,[16] and tellurium species should have the strongest ChB properties.[17] In this respect, several studies on tellurium compounds in solution[18] focused on Te···O,[19] Te···N,[20] Te···Ch,[21] and Te···Pnictogen[22] interactions (Fig. 2, top). Despite their detection in some cases in the solid state,[4a,23] Te···F interactions have been scarcely studied in solution.[24] In particular, Zhao and Gabbaï reported the recognition of a fluoride anion by 2-boronylnaphtyl telluronium; however the presence of a covalent bond was finally established with such bidentate compounds.[24a]

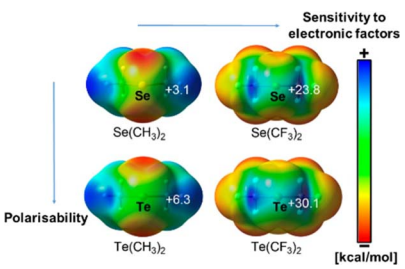

Fig. 1 Electrostatic potential maps of selected chalcogen derivatives revealing the electropositive areas, called σ-holes. Adapted from ref. 5.

[a]*LASYROC, UMR 7177, University of Strasbourg, 1 Rue Blaise Pascal, 67000 Strasbourg, France. E-mail: ppale@unistra.fr; vmamane@unistra.fr*

[b]*Université de Lorraine, CNRS, CRM2, F-54000 Nancy, France*

† Electronic supplementary information (ESI) available: Experimental procedures, characterisation data and NMR spectra; VT NMR spectra and coupling constants; computed conformational analysis and $V_{s,max}$ data; computed NMR data; methodology for the determination of thermodynamic parameters. See DOI: https://doi.org/10.1039/d3sc00849e

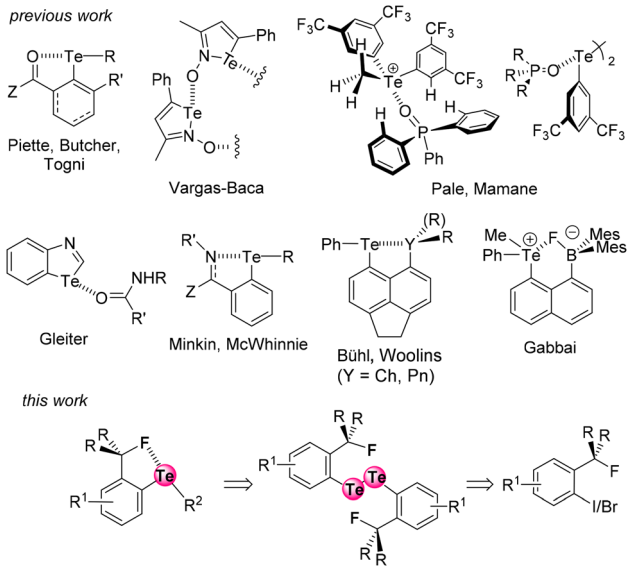

Fig. 2 The known noncovalent interactions involving tellurium atoms, and the Te···F interaction described here.

This context urges us to identify Te···F interaction and to characterize the corresponding properties.

In continuation of our recent XB and ChB studies and applications in medicinal chemistry,[25] enantioseparation,[26] and organocatalysis,[19b,27] we have now designed two series of fluorinated *ortho*-tolyl telluride derivatives to identify Te···F interactions and to characterize their corresponding properties. We report here the first evidence of a Te···F interaction (ChB) in solution, as well as an evaluation of its strength (Fig. 2, bottom).

Results and discussion

Probe design

The choice of fluorinated *ortho*-tolyl telluride derivatives as a Te···F probe was motivated by three factors. First, a Te···F interaction should influence the rotational barrier of the fluoromethyl substituent and related groups. Second, the probe provides an opportunity to monitor the presence of rotational isomers by combining ^{19}F and ^{125}Te NMR, and thus to evaluate the strength of the Te···F interaction. Finally, Te σ-hole(s) can be tuned by using appropriate electron-withdrawing or -donating substituent(s) either on the tolyl moiety or on the other Te substituent (R^1 and R^2 respectively in Fig. 2, bottom left). The simplest *ortho*-fluoromethylphenyl telluride (CH_2F series) must exhibit at least two rotamers: one (*syn*-CH_2F) where tellurium and fluoride atoms are close to one another and a second (*anti*-CH_2F) in which the fluoride could be far from the tellurium atom (Fig. 3A). Obviously, an intramolecular Te···F interaction would only exist in *syn*-CH_2F and, if so and strong enough, this interaction could shift the conformational equilibrium towards this *syn*-conformer. Furthermore, the latter should exhibit different chemical shifts in ^{19}F and ^{125}Te NMR due to electron density transfer from F to Te depending on the Te···F interaction strength. Coupling constants could also be

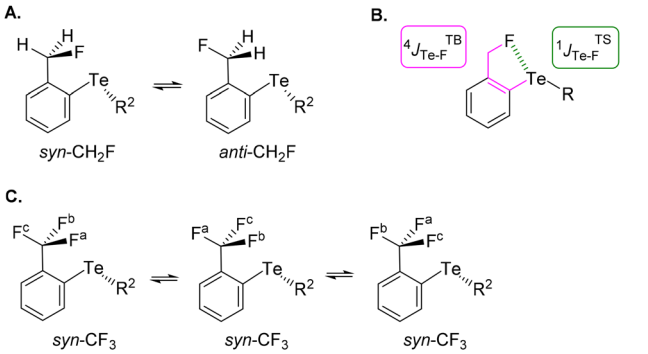

Fig. 3 (A) The more stable *syn* and *anti* conformations for the CH_2F series. (B) Through bond (TB) and through space (TS) coupling for the *syn* conformation in the CH_2F series. (C) Permanent *syn* conformation in the CF_3 series.

helpful because both ^{19}F and ^{125}Te exhibit $\frac{1}{2}$ nuclear spin. In addition to the through-bond coupling constant ($^4J^{TB}_{Te-F}$), a through-space contribution ($^1J^{TS}_{Te-F}$) to the overall coupling constant ($^4J_{Te-F}$) should arise in *syn*-CH_2F if Te···F interaction is present (Fig. 3B).[28] Therefore, ^{19}F and ^{125}Te NMR monitoring could reveal such differences and provide information on the conformational equilibrium and its evolution.

In contrast, the *ortho*-trifluoromethylphenyl telluride (CF_3 series) will always have one fluoride facing or close to the tellurium atom (Fig. 3C). Therefore, depending on the strength of the Te···F interaction, two possibilities could arise: this interaction could either lock the rotation of the CF_3 group and thus make the fluoride atoms non-equivalent in NMR, or could be averaged over the CF_3 group.

Synthesis

To address these issues, we prepared two series of *ortho*-tolyl tellurides bearing either a fluoromethyl or a trifluoromethyl group (Schemes 1 and 2). Starting from fluoromethyl-2-iodobenzene **1**, iodine–lithium exchange followed by trapping with grey tellurium gave the corresponding lithium telluride,[29] which upon quenching under air provided in high yield the corresponding diaryl ditelluride **2** (ref. [30]) (Scheme 1, top). Applying the same strategy to iodo-2-trifluoromethylbenzene **3**

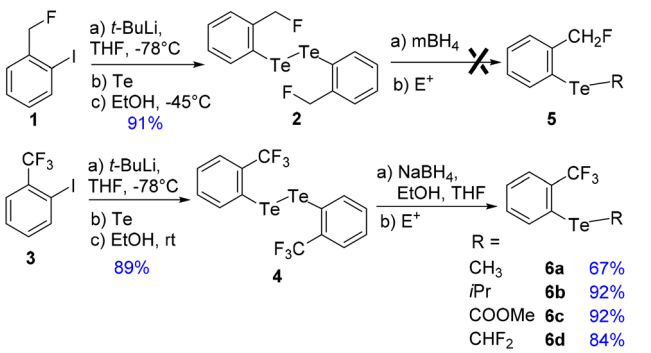

Scheme 1 Synthesis of a series of fluorinated alkyl aryl tellurides.

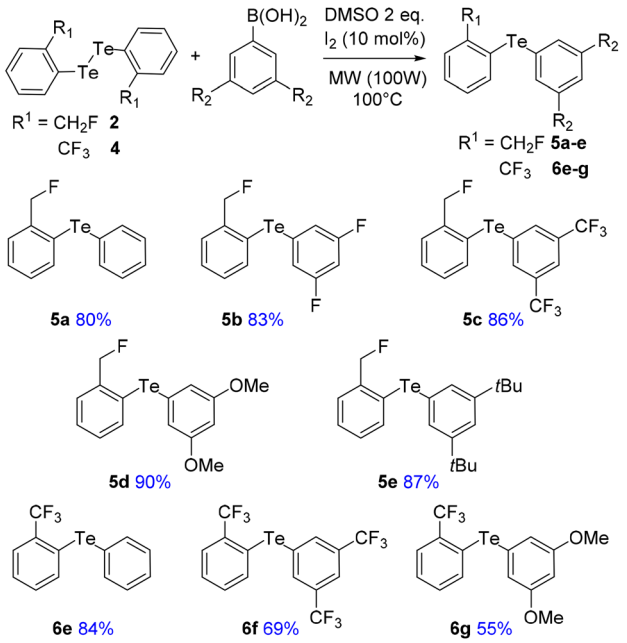

Scheme 2 Synthesis of a series of fluorinated diaryl tellurides.

gave the trifluoromethyl analogue **4** in similar yield.[19a] Upon reductive cleavage and trapping of the resulting tellurolate by electrophiles, ditelluride **2** afforded mixtures in which the expected tellurides **5** could not be detected, independent of the nature of the borohydride or electrophile (Scheme 1, top). In contrast, the treatment of ditelluride **4** with $NaBH_4$ and subsequent electrophilic quenching readily gave the expected alkyl aryl tellurides **6a–c** with good to high yields. Under these conditions, using CF_2Br_2 as the electrophile resulted only in the debrominated product **6d** (Scheme 1, bottom).

A more general route to both tellurides **5** and **6** was achieved by a microwave-promoted coupling reaction with various arylboronic acids (Scheme 2).[31] To tune the expected ChB intensity, a series of boronic acid derivatives carrying electron-rich or electron-poor substituents was employed in this coupling to provide the corresponding diaryl tellurides **5a–e** and **6e–g** in good to high yields. These compounds could be stored at 4 °C for several months without degradation. Moreover, the diaryldditellurides showed good stability in solution at room temperature for several days with no particular precautions. In contrast, alkyl aryl tellurides **6a–d** were very sensitive to oxygen and light, causing rapid decomposition in solution with the formation of a grey metallic deposit, probably corresponding to tellurium(0).[32] Unfortunately, all of the prepared tellurides **5** and **6** were viscous oils that could not be crystallized.

Electrostatic surface potential (ESP) analysis

For ESP analysis, compounds **5a**, **5c**, **6e**, and **6f** were chosen as representative members of respectively the CH_2F and CF_3 series. Their molecular geometries were optimized by DFT (B3LYP/Def2TZVPP, see ESI† Section IV.B for details). As anticipated for the CH_2F series, the *syn*-CH_2F and *anti*-CH_2F conformations were found to be the most stable ones among all possible conformations for both **5a** and **5c** (see ESI Fig. S10 and Table S8†). Coherently, only one stable conformation was detected for **6e** and **6f** (Fig. 3C, S10 and Table S9†). The $V_{s,max}$ extrema were then characterized for each conformation of **5a** and **5c** (see ESI, Tables S8 and S9 and Fig. S11†). Interestingly, only one σ-hole was detected in the *syn* conformers in the elongation of the bond between Te and the aromatic group bearing CH_2F. The other σ-hole that was expected to be facing the fluorine atom could not be characterized. The latter σ hole could be detected in the *anti* conformer, however. These results suggest a possible through-space electron delocalization from fluorine to a tellurium σ-hole in the *syn* conformer. This hypothesis was further supported by the topological analysis of the DFT calculated electron density, where a bond path is observed between F and Te atoms with a small but non-negligible delocalization index of about 0.065 (see ESI Fig. S12 and Table S10†). Similar data were obtained with compounds **6e** and **6f** (see ESI Table S10†).

Te···F interaction in solution

The mono- and tri-fluorotolyl tellurides **5a–e** and **6a–g**, as well as their ditelluride precursors **2** and **4**, were then studied in solution, using ^{19}F and ^{125}Te NMR to probe the presence or absence of σ-hole Te···F interactions (see spectra in ESI, Section V†).

The trifluorotolyl tellurium derivatives **6a–g** exhibit similar chemical shifts in ^{19}F NMR (−61 ± 1 ppm), but a large shift range in ^{125}Te NMR (369–795 ppm) (Table 1). The latter are nevertheless typical of divalent tellurides,[33] as observed in the ^{19}F and ^{125}Te NMR spectra of **4** (−60.5 ppm and 438.1 ppm, respectively). The ^{125}Te signal appears as a quadruplet, indicating a $^4J_{Te-F}$ coupling with the three fluorine atoms of the trifluoromethyl group. This quadruplet also reveals the magnetic equivalence of these fluorine atoms, and thus the free rotation of the trifluoromethyl group at room temperature and even at −80 °C. Interestingly, these $^4J_{Te-F}$ coupling constants (94–154 Hz, Table 1) are far lower than those observed for covalent Te–F bonds (~950 Hz).[24,34] Nevertheless, they are two to four times higher than $^3J_{Te-F}$ coupling values in the 2,6-difluorophenylditelluride **7** (45 Hz), used for comparison purposes. Such a counter-intuitive difference was observed in various fluorinated compounds[35] and in HBs involving fluorine.[36] The underlying phenomenon was ascribed to through-space orbital overlap,[37] and non-linearly correlated to the distance of the interacting atoms, and thus to the strength of the interaction.[35b] The latter could be assessed from the good linear correlation between ^{19}F chemical shifts (δ_F) and $^4J_{Te-F}$ coupling constants (Fig. 4). This correlation revealed that more shielded δ_F correspond to higher $^4J_{Te-F}$ values, and therefore to stronger interactions.

Furthermore, the ^{19}F NMR chemical shifts of **4** and **6a–g** (−61 ± 1 ppm) were higher than that of trifluorotoluene **8** (−63.8 ppm), independent of the Te substituent. This deshielding is mostly due to the presence of tellurium and indicates a modification of fluorine polarization, as expected from an interaction between the F lone pair and Te σ-holes. These combined observations strongly suggest the presence of noncovalent Te···F interactions in this series of Te compounds.

Table 1 ^{125}Te and ^{19}F NMR chemical shifts and Te–F coupling constants from tellurium derivatives **4** and **6a–g** compared to the ditelluride **7** and trifluorotoluene **8**[a]

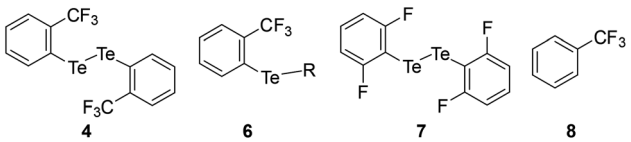

Tellurium (R)	δ_{Te} (ppm)	δ_F (ppm)	$^3J_{Te-F}$ (Hz)	$^4J_{Te-F}$ (Hz)	$^5J_{C-F}$ (Hz)
4	438.1	−60.5	—	170.2	—
6a (CH_3)	369.4	−62.0	—	153.3	2.98
6b (iPr)	720.7	−60.7	—	99.5	1.74
6c (COOMe)	795.5	−60.0	—	107.4	2.87
6d (CF_2H)	-[b]	−60.3	—	95.9[c]	2.67
6e (Ph)	728.2	−61.8	—	162.5	—
6f (3,5-$(CF_3)_2$Ph)	779.5	−61.1	—	146.9	—
6g (3,5-$(MeO)_2$Ph)	760.1	−61.8	—	167.5	—
7	215.6	−86.2	45.5	—	—
8	—	−63.8	—	—	—

[a] Conditions: tellurium species (5–20 mM) in $CDCl_3$ at 25 °C. [b] The product decomposed during the acquisition of the ^{125}Te NMR spectrum. [c] Measured on the ^{19}F spectrum.

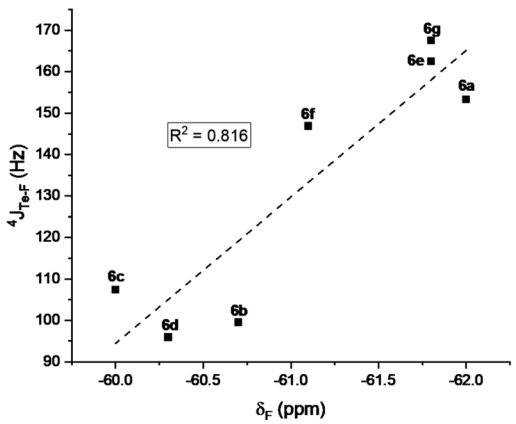

Fig. 4 Correlation between the ^{19}F NMR chemical shifts of the tellurides **6a–g** and $^4J_{Te-F}$ coupling constants.

Unexpected observations in ^{13}C NMR corroborate this possibility. The alkyl aryl tellurides **6a–d** exhibit what appears as a $^5J_{C-F}$ coupling between the Te-bound alkyl, aryl or carboxylate carbon bonded to the tellurium atom and the fluorine atoms (Fig. 5). Despite the large number of bonds separating them and the presence of the tellurium atom, the observed coupling constants were unexpectedly high (1.74–2.98 Hz; see Table 1). These values are usually typical of $^3J_{C-F}$ couplings.[38] Such coupling[39] could be due to noncovalent Te···F interactions, and if so, the Te σ-hole involved should impose a configuration in which the Te substituent would be aligned with the Te···F interaction in an *anti* position (see the drawing in Fig. 6).

To verify this hypothesis, a ^{1}H–^{19}F HOESY NMR experiment was performed with the methyl-substituted telluride **6a** (Fig. 6). This experiment revealed that the methyl is not close to the CF_3 group, whereas the latter is close to the *ortho*-proton of the phenyl moiety. Therefore, the methyl group should be oriented away from the CF_3 group in solution. Such observations further corroborate the presence of a Te···F interaction.

The monofluorotolyl tellurides **5a–e** were then investigated under the same NMR conditions (Table 2). ^{125}Te NMR chemical shifts (345–645 ppm) were again in the classical range for divalent tellurides.[33] As for the CF_3 series, the ^{19}F NMR chemical shifts of **2** and **5a–e** (−204 ± 1 ppm) were higher than that of the reference compound **9** (−206.1 ppm). A long-range $^4J_{Te-F}$ coupling between the fluorine and tellurium atoms was also observed as a doublet in this series, with similar values (104.6–129.6 Hz). The latter are nevertheless lower than in the CF_3 series, as are the ^{125}Te chemical shifts (see **5a** *vs.* **6e**, **5c** *vs.* **6f**, **5d** *vs.* **6g** and **2** *vs.* **4**). Both facts further support the presence of a Te···F σ-hole-based interaction for the same reason.

Because the deepness of a σ-hole is directly affected by adjacent electron-withdrawing or -donating substituent(s) (see Fig. 1), we attempted to tune Te σ-holes by selecting typical substituents at the *meta* position of the Te aryl moiety (**5b–e** *vs.* **5a**) in this more structurally homogeneous series.

Rewardingly, the electronic effect (σ_m) of these meta substituents could clearly be correlated to ^{125}Te chemical shifts

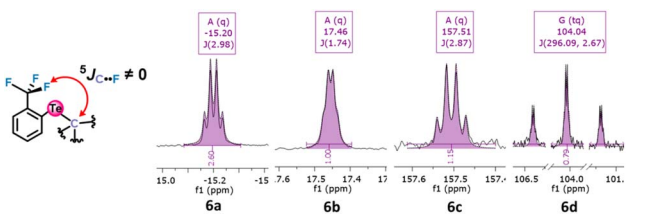

Fig. 5 Fragments of tellurides **6a–d** ^{13}C NMR spectra revealing $^5J_{C-F}$ due to coupling between the carbon bonded to the tellurium atom and the fluorine atoms.

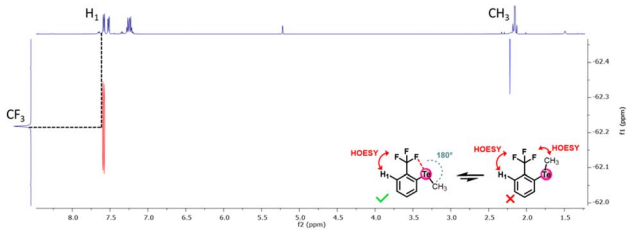

Fig. 6 HOESY spectrum of telluride **6a** in CD_2Cl_2.

Table 2 ^{125}Te and ^{19}F NMR chemical shifts and Te–F coupling constants from tellurium derivatives **2** and **5a–e** compared to the monofluorotoluene **9**[a]

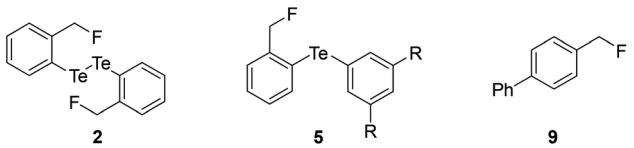

Tellurium (R)	δ_{Te} (ppm)	δ_F (ppm)	$^4J_{Te-F}$ (Hz)
2	345.6	−203.2	129.6
5a (H)	596.4	−205.3	110.4
5b (F)	644.8	−204.3	108.7
5c (CF_3)	645.1	−202.3	127.0
5d (OMe)	622.8	−205.3	108.8
5e (*t*Bu)	594.3	−205.5	108.5
9	—	−206.1	—

[a] Conditions: tellurium species (20 mM) in $CDCl_3$ at 25 °C.

(Fig. 7A). Moreover, ^{19}F chemical shifts correlated with the $^4J_{Te-F}$ coupling constants (Fig. 7B) and showed that the more electron-withdrawing substituent induced the largest $^4J_{Te-F}$ coupling, as expected for a σ-hole-based interaction. These effects confirmed that the $^4J_{Te-F}$ value represents a measure of the strength of the noncovalent Te···F interaction.

Contribution of the Te···F ChB to the overall $^4J_{Te-F}$

Two different studies were performed in order to confirm the role of the Te σ-hole in the Te···F interaction and to estimate the ChB contribution to the overall coupling constant.

In the first study, the lithium tellurolate intermediate **10-TeLi**, where the negative charge on Te was expected to reduce the involvement of its σ-hole in the Te···F interaction, was prepared (Scheme 3). The characterization of **10-TeLi** by NMR and in particular the determination of the Te–F coupling constant should provide an approximate assessment of the through-space coupling due to chalcogen bonding.

Lithium tellurolate **10-TeLi** was obtained by slow decomposition of **10-TeBH$_3$Li**. The latter was generated by the reaction of ditelluride **4** with an excess of $LiBH_4$ in THF.[40] The decomposition of **10-TeBH$_3$Li** to **10-TeLi** was monitored by ^{19}F NMR in THF-d_8 (Scheme 3 and ESI† for full characterization). Almost full conversion was observed after 16 days with complete disappearance of the boron signal of **10-TeBH$_3$Li** in ^{11}B NMR

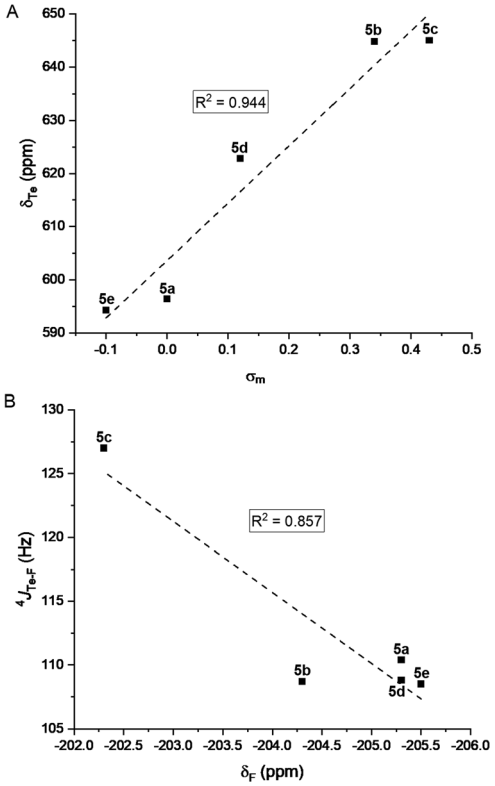

Fig. 7 (A) Correlation between the ^{125}Te NMR chemical shifts of the tellurides **5a–e** and Hammett parameter (σ_m). (B) Correlation between $^4J_{Te-F}$ coupling constants and ^{19}F NMR chemical shifts.

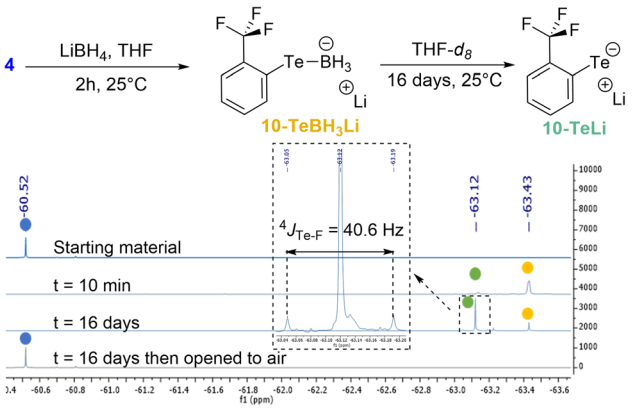

Scheme 3 Preparation of lithium tellurolate **10-TeLi** and ^{19}F NMR monitoring (color code: **4** in blue, **10-TeBH$_3$Li** in yellow and **10-TeLi** in green).

and the appearance of a new ^{125}Te signal for **10-TeLi** (see the ESI†).[41] Moreover, ditelluride **4** was recovered by oxidation of **10-TeLi** after opening the NMR tube to air. These observations proved that **10-TeLi** was formed after 16 days. The Te–F coupling constant of 40.6 Hz measured for **10-TeLi** was much lower than the $^4J_{Te-F}$ values observed for tellurides **6a–g** (Table 1). Such a large difference between the telluride and the tellurolate should at least partly reveal the through-space

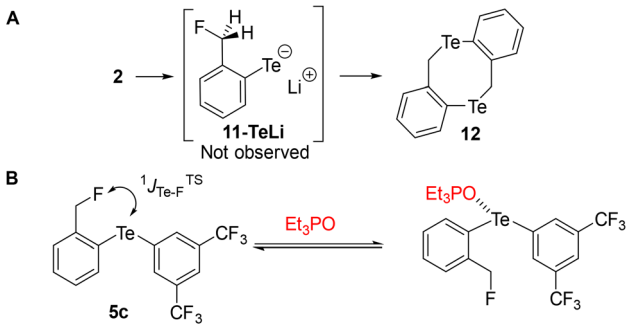

Scheme 4 (A) Attempted preparation of tellurolate **11-TeLi**. (B) Competition experiments between **5c** and Et_3PO.

contribution and thus indicates a contribution of the Te···F ChB to the overall $^4J_{Te-F}$ in compounds **6a–g**.

Similarly, we attempted to form the analogous tellurolate **11-TeLi** but all attempts failed, probably because it dimerized to tellurocine **12** (Scheme 4A).[30]

In the second study, the $^4J_{Te-F}$ evolution of tellurides in the presence of Et_3PO Lewis base was investigated by NMR. The tellurides were expected to form an intermolecular Te···O interaction in competition with the intramolecular Te···F ChB with a direct influence on $^4J_{Te-F}$ (Scheme 4B). This strategy was tested on telluride **5c** with the strongest Te···F ChB, and to avoid a possible HB between Et_3PO and $CDCl_3$, competition experiments were performed in deuterated cyclohexane.[19a] Large variations of $^4J_{Te-F}$ were obtained after the addition of 1, 5 and 10 equiv. of Et_3PO ($\Delta^4J_{Te-F} = -7.8$, -24.3 and -32.8 Hz, respectively) and a plateau (~33 Hz) was reached between 10 and 20 equiv. of Lewis base (see the ESI† for details).

At this plateau, the intramolecular Te···F interaction was completely replaced by the intermolecular Te···O interaction. Therefore, the difference of about 33 Hz should reflect the contribution of the Te···F ChB to the overall $^4J_{Te-F}$ value.

This strategy was unsuccessful when applied to telluride **6f**. Indeed, no modification of $^4J_{Te-F}$ was observed after the addition of 1 equiv. of Et_3PO and only small variations were observed when 5 or 10 equiv. were employed ($\Delta^4J_{Te-F} = -3.7$ and -5.9 Hz, respectively) (see the ESI† for details). These variations represent only 2.4 and 3.9% of the $^4J_{Te-F}$ value before the addition of the Lewis base, suggesting that the Te···F interaction is strong enough in telluride **6f** to outweigh the competition from an intermolecular Lewis base such as Et_3PO.

Evaluating the strength of Te···F interaction in solution for compounds 5

As determined above, the measured $^4J_{Te-F}$ coupling may reflect the noncovalent Te···F interaction strength, but its value is averaged over the various conformations. Based on our conformational analysis, the *syn* and *anti* conformers are the major ones; we can reasonably assume a two state equilibrium model in which the $^4J_{Te-F}$ coupling results from the relative proportion of each conformation contribution $^4J_{Te-F(syn)}$ and $^4J_{Te-F(anti)}$ (eqn (1)); χ_{syn} is a temperature-dependent variable representing the relative population of the *syn* conformer).

$$^4J_{Te-F} = \chi_{syn}(^4J_{Te-F(syn)}) + (1 - \chi_{syn})(^4J_{Te-F(anti)}) \quad (1)$$

This expression can be inserted into eqn (2), which defines the *anti–syn* equilibrium constant K_A to give eqn (3).

$$K_A = \chi_{syn}/(1 - \chi_{syn}) \quad (2)$$

$$K_A = (^4J_{Te-F} - {}^4J_{Te-F(anti)})/(^4J_{Te-F(syn)} - {}^4J_{Te-F}) \quad (3)$$

The Gibbs free energy of this equilibrium is thus expressed as a function of coupling constants and of temperature (eqn (4)).

$$\Delta G = \Delta H - T\Delta S = -RT\ln K_A = -RT\ln\left[\left({}^4J_{Te-F} - {}^4J_{Te-F(anti)}\right)\right] \quad (4)$$

To evaluate the $^4J_{Te-F}$ values as a function of the conformation, relativistic DFT calculations were performed on each conformer. These calculations provided large negative values for $^4J_{Te-F}$ (-249 ± 4 Hz for **5a–c**; -164 ± 2 Hz for **6e** and **6f**) and a much smaller positive value for $^4J_{Te-F(anti)}$ (+19–20 Hz) (see ESI Section IV.D, Table S11†). Surprisingly, a related study with fluoroseleno compounds suggested that $^4J_{Te-F(anti)}$ was approximately zero because no Se···F coupling was detected in selenolate **11-SeLi**, which was considered to be in an *anti* conformation due to electronic repulsion.[14] This could not be confirmed on the analogous tellurolate **11-TeLi** because of its instability (Scheme 4A).[30] We nevertheless performed relativistic DFT calculations for **11-TeLi**, along all the C–C–C–F torsion angles from the *anti* to the *syn* conformer. The resulting data showed that $^4J_{Te-F(anti)}$ remains relatively constant (20 ± 10 Hz) from the *anti* to a 90° arrangement and then sharply decreases to -130 Hz for the *syn* conformer (see ESI Section IV.D and Fig. S13†). All of the computed data showed that $^4J_{Te-F(anti)}$ is close to 20 Hz, independent of the telluronium structure, the tellurolate **11-TeLi**, the ditelluride **2** and the monotellurides **5a** and **5c** (see ESI Section IV.D, Fig. S13 and Table S11†).

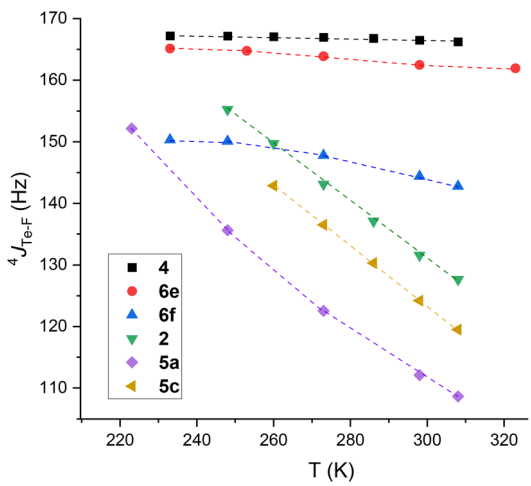

Fig. 8 Evolution of $^4J_{Te\cdots F}$ of trifluorotolyl (**2**, **6e** and **6f**) and monofluorotolyl (**4**, **5a** and **5c**) derivatives as a function of temperature.

Table 3 Thermodynamic parameters of the *anti–syn* equilibrium of tellurium derivatives **2**, **5a** and **5c**[a]

Compound	$\Delta H \approx E_{Te\cdots F}$ (kJ mol^{-1})	ΔS (J K^{-1} mol^{-1})	ΔG^{298} (kJ mol^{-1})
2	−7.6 to −6.3	−21.3 to −15.5	−1.2 to −1.7
5a	−4.4 to −3.0	−20.7 to −17.0	+1.6 to +2.1
5c	−10.6 to −9.1	−29.5 to −22.4	−1.8 to −2.4

[a] See ESI, Table S7 for full data.

To obtain experimental data on $^4J_{Te-F}$, and in order to assess thermodynamic parameters, typical mono- and tri-fluorotolyl tellurium derivatives (**2**, **4**, **5a**, **6e**, **5c** and **6f**) were examined by variable temperature (VT) NMR from 233 to 308 K (Fig. 8 and ESI, Section III.A and B†). The trifluoro compounds were studied as models with permanent *syn* conformations in order to verify the non-dependency of $^4J_{Te-F(syn)}$ on temperature.

Low variations of $^4J_{Te-F}$ were obtained for the trifluorotolyl derivatives (variation for **4**: 0.7%; **6e**: 2.6%; **6f**: 6.9%) proving that $^4J_{Te-F}$ is almost independent of temperature (see ESI Section III.A† for complete data). In contrast, the monofluorotolyl compounds (**2**, **5a** and **5c**) showed large variations (Δ^4J_{Te-F} up to 44 Hz), as expected from temperature-dependent modification of the *anti–syn* equilibrium. Interestingly, the highest value was observed for the 3,5-bis(trifluoromethyl) phenyl derivative **5c** that exhibits the largest Te σ-hole (Fig. 8 and ESI, Section III.B†). Similarly, δ_F displayed a net deshielding upon decreasing the temperature for the monofluorotolyl derivatives ($\Delta\delta_F \sim 4$ ppm, Tables S4–S6 in ESI†), but a slight shielding for the trifluorotolyl analogs ($\Delta\delta_F \sim 0.5$ ppm) (Tables S1–S3 in ESI†). Such effects are in line with an increased electron density transfer from an F lone pair to the Te σ-hole in the monofluorotolyl series, as expected from increasing predominance of the *syn* conformer.

Based on the results at low temperature, the enthalpy of the *anti–syn* equilibrium seems to be mostly driven by the Te···F interaction. Therefore, this enthalpy can be estimated from the energy of the Te···F interaction using eqn (5):

$$\Delta H \approx E_{Te\cdots F} \quad (5)$$

From the experimental VT NMR data, the ΔH and ΔS of eqn (4) were determined as follows. Assuming a two state model, we first determined the values of $^4J_{Te-F(anti)}$ and $^4J_{Te-F(syn)}$ that give the best linearity of $-RT\ln K_A$ as a function of T. Due to poor convergence, one of the two parameters was fixed while refining the second one. We thus chose to solve eqn (4) for two different fixed values of $^4J_{Te-F(anti)}$, namely −20 Hz and +20 Hz because these values represent the average theoretical calculations for $^4J_{Te-F(anti)}$ (see above) and because positive and negative coupling constants were calculated for non-*syn* conformations. The optimal value of $^4J_{Te-F(syn)}$ was then determined, leading to a linear fit and values of ΔH and ΔS that were obtained as intervals corresponding to the positive and negative estimated values of $^4J_{Te-F(anti)}$ (see ESI Section III.C and Table S7†). The estimated values of ΔH and ΔS were then used to calculate $E_{Te\cdots F}$ and ΔG^{298} (Table 3). For compounds **2** and **5c**, the obtained negative ΔG^{298} values for the *anti* ⇌ *syn* equilibrium indicated a favorable shift towards the *syn* conformer, and thus confirmed the preference in solution for the conformer exhibiting a σ-hole Te···F interaction. In contrast, the positive value of ΔG^{298} obtained for compound **5a** indicated that the *anti* conformer is the major component in solution at room temperature. This result revealed the strong influence of the presence of electron-withdrawing substituents, which increase the deepness of the Te σ-hole, and thus the Te···F interaction, as recently demonstrated for related σ-hole interactions involving tellurium atoms.[19a,b]

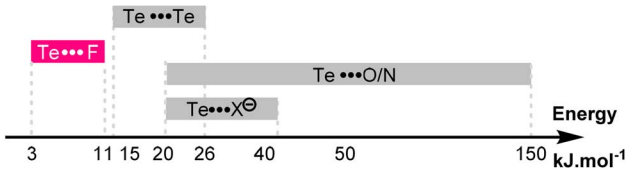

Fig. 9 Energy range of the known noncovalent interactions involving the tellurium atom and of the Te···F interaction reported here.

This effect is also reflected by the more negative entropy of compound **5c** compared to **5a** (−26.0 *vs.* −18.9 J K^{-1} mol^{-1}). Here again, the increased deepness of the Te σ-hole strengthens the Te···F interaction, which in turn increases the proportion of the *syn* conformer and reduces the molecular degree of freedom. The energies of these Te···F interactions are modest (−3 to −11 kJ mol^{-1}), and slightly lower than the well-known Te···Te interactions.[42] The Te···F interactions described here are thus in the lower range of the already known noncovalent interactions involving a tellurium atom (Fig. 9).

Conclusions

In conclusion, after having prepared new fluoro- and trifluoro tellurium derivatives, we demonstrated the presence of noncovalent Te···F interactions through the σ-holes on tellurium and their importance in solution as indicated by ^{19}F and ^{125}Te NMR studies. The various effects reported here established the presence of ChB between Te and F as schematically shown in Fig. 3B.

By variable temperature experiments, we were even able to evaluate the intensity of such noncovalent Te···F interactions (−3 to −11 kJ mol^{-1}). The identification of noncovalent Te···F interactions reported here should provide new opportunities in organic chemistry, especially in organocatalysis, in drug design and in biology. Further work in these areas is underway in our group.

Data availability

Experimental and computational data associated with this work are provided in the accompanying ESI.†

Author contributions

RW and LG carried out the experiments. EA performed the computational studies. RW, PP and VM designed the project. PP and VM co-wrote the manuscript. VM co-wrote and edited the ESI.† RW and EA co-wrote the ESI† and contributed to writing the manuscript.

Conflicts of interest

There are no conflicts to declare.

Acknowledgements

This research was funded by the International Center Frontier Research in Chemistry (icFRC), the LabEx CSC (ANR-10-LABX-0026 CSC) and the French National Research Agency (ANR-21-CE07-0014). RW thanks the LabEx CSC, Strasbourg, for a PhD fellowship and LG thanks the ANR for a PhD fellowship. We thank the EXPLOR mesocenter for providing access to their computing facility (project 2021CPMXX2483) and the NMR service (B. Vincent) of the LeBel Federation FR2010 for the easy access to the spectrometers and for advice. EA thanks Dr Axel Gansmüller for fruitful discussions.

References

1 (*a*) P. Politzer, J. S. Murray and T. Clark, *Phys. Chem. Chem. Phys.*, 2013, **15**, 11178–11588; (*b*) A. Bauzá, T. J. Mooibroek and A. Frontera, *ChemPhysChem*, 2015, **16**, 2496–2517.

2 G. Cavallo, P. Metrangolo, R. Milani, T. Pilati, A. Priimagi, G. Resnati and G. Terraneo, *Chem. Rev.*, 2016, **116**, 2478–2601.

3 For recent developments in XB applications in biology and in organic chemistry, see: (*a*) G. Berger, P. Frangville and F. Meyer, *Chem. Commun.*, 2020, **56**, 4970–4981; (*b*) R. L. Sutar and S. M. Huber, *ACS Catal.*, 2019, **9**, 9622–9639.

4 ChB has been sparingly investigated in the last decade, see: (*a*) P. Scilabra, G. Terraneo and G. Resnati, *Acc. Chem. Res.*, 2019, **52**, 1313–1324; (*b*) N. Biot and D. Bonifazi, *Coord. Chem. Rev.*, 2020, **413**, 213243; (*c*) R. Hein and P. D. Beer, *Chem. Sci.*, 2022, **13**, 7098.

5 A. Frontera and A. Bauza, *Int. J. Mol. Sci.*, 2022, **23**, 4188.

6 C. B. Aakeröy, D. L. Bryce, G. R. Desiraju, A. Frontera, A. C. Legon, F. Nicotra, K. Rissanen, S. Scheiner, G. Terraneo, P. Metrangolo and G. Resnati, *Pure Appl. Chem.*, 2019, **91**, 1889–1892.

7 (*a*) M. R. Scholfield, C. M. Vander Zanden, M. Carter and P. S. Ho, *Protein Sci.*, 2013, **22**, 139–152; (*b*) P. S. Ho, *Future Med. Chem.*, 2017, **4**, 637–640.

8 (*a*) M. Iwaoka and N. Isozumi, *Molecules*, 2012, **17**, 7266–7283; (*b*) K. Kriz, J. Fanfrik and M. Lepsik, *ChemPhysChem*, 2018, **19**, 2540–2548.

9 E. R. T. Tiekink, *Dalton Trans.*, 2012, **41**, 6390–6395.

10 (*a*) P. Shah and A. D. Westwell, *J. Enzyme Inhib. Med. Chem.*, 2007, **22**, 527–540; (*b*) *Fluorine in Medicinal Chemistry and Chemical Biology*, ed. I. Ojima, Wiley-Blackwell, 2009.

11 W. Pietrus, R. Kafel, A. J. Bojarski and R. Kurczab, *Molecules*, 2022, **27**, 1005–1019.

12 (*a*) The actual presence of XBs with the F atom is still a matter of debate; see ref. 2 and: P. Metrangolo, J. S. Murray, T. Pilati, P. Politzer, G. Resnati and G. Terraneo, *Cryst. Growth Des.*, 2011, **11**, 4238–4246; (*b*) K. Eskandari and M. Lesani, *Chem.–Eur. J.*, 2015, **21**, 4739–4746; (*c*) S. Scheiner, *J. Phys. Chem. A*, 2020, **124**, 7290–7299; (*d*) S. A. Harry, S. Vemulapalli, T. Dudding and T. Lectka, *J. Org. Chem.*, 2022, **13**, 8413–8419.

13 K. Grollier, A. Taponard and T. Billard, *Eur. J. Org. Chem.*, 2020, **2020**, 6943–6954.

14 For a study on the Se–F interaction, see: M. Iwaoka, H. Komatsu, T. Katsuda and S. Tomoda, *J. Am. Chem. Soc.*, 2002, **124**, 1902–1909.

15 Pauling electronegativity of halogens: F 4.0, Cl 3.0, Br 2.8, and I 2.5, and of chalcogens: O 3.5, S 2.5, Se 2.4, and Te 2.1.

16 P. Politzer, P. Lane, M. C. Concha, Y. Ma and J. S. Murray, *J. Mol. Model.*, 2007, **13**, 305–311.

17 B. Zhou and F. P. Gabbai, *Chem. Sci.*, 2020, **11**, 7495–7500.

18 P. Pale and V. Mamane, *ChemPhysChem*, 2023, **24**, e202200481.

19 (*a*) R. Weiss, E. Aubert, L. Groslambert, P. Pale and V. Mamane, *Chem.–Eur. J.*, 2022, **28**, e202200395; (*b*) R. Weiss, E. Aubert, P. Pale and V. Mamane, *Angew. Chem., Int. Ed.*, 2021, **60**, 19281–19286; (*c*) H. Nishiyama, F. Zheng, S. Inagi, H. Fueno, K. Tanaka and I. Tomita, *Polym. Chem.*, 2020, **11**, 4693–4698; (*d*) S. Mehrparvar, C. Wölper, R. Gleiter and G. Haberhauer, *Angew. Chem., Int. Ed.*, 2020, **59**, 17154–17161; (*e*) L. Chen, J. Xiang, Y. Zhao and Q. Yan, *J. Am. Chem. Soc.*, 2018, **140**, 7079–7082; (*f*) E. Pietrasiak and A. Togni, *Organometallics*, 2017, **36**, 3750–3757; (*g*) P. C. Ho, P. Szydlowski, J. Sinclair, P. J. W. Elder, J. Kübel, C. Gendy, L. M. Lee, H. Jenkins, J. F. Britten, D. R. Morim and I. Vargas-Baca, *Nat. Commun.*, 2016, **7**, 11299; (*h*) P. R. Prasad, K. Selvakumar, H. B. Singh and R. J. Butcher, *J. Org. Chem.*, 2016, **81**, 3214–3226; (*i*) M. Baiwir, G. Llabres, J. Denoel and J.-L. Piette, *Mol. Phys.*, 1973, **25**, 1–7.

20 (*a*) T. Glodde, Y. V. Vishnevskiy, L. Zimmermann, H.-G. Stammler, B. Neumann and N. W. Mitzel, *Angew. Chem., Int. Ed.*, 2021, **60**, 1519–1523; (*b*) M. Hejda, D. Duvinage, E. Lork, R. Jirásko, A. Lyčka, S. Mebs, L. Dostál and J. Beckmann, *Organometallics*, 2020, **39**, 1202–1212; (*c*) I. D. Sadekov, V. I. Minkin, A. V. Zakharov, A. G. Starikov, G. S. Borodkin, S. M. Aldoshin, V. V. Tkachev, G. V. Shilov and F. J. Berry, *J. Organomet. Chem.*, 2005, **690**, 103–116; (*d*) A. G. Maslakov, W. R. McWhinnie, M. C. Perry, N. Shaikh, S. L. W. McWhinnie and T. A. Hamor, *J. Chem. Soc., Dalton Trans.*, 1993, 619–624.

21 (*a*) M. Bühl, F. R. Knight, A. Křístková, I. M. Ondík, O. L. Malkina, R. A. M. Randall, A. M. Z. Slawin and

J. D. Woollins, *Angew. Chem., Int. Ed.*, 2013, **52**, 2495–2498; (*b*) F. R. Knight, L. M. Diamond, K. S. Athukorala Arachchige, P. Sanz Camacho, R. A. M. Randall, S. E. Ashbrook, M. Bühl, A. M. Z. Slawin and J. D. Woollins, *Chem.–Eur. J.*, 2015, **21**, 3613–3627; (*c*) M. W. Stanford, F. R. Knight, K. S. A. Arachchige, P. S. Camacho, S. E. Ashbrook, M. Bühl, A. M. Z. Slawin and J. D. Woollins, *Dalton Trans.*, 2014, **43**, 6548–6560.

22 (*a*) A. Nordheider, E. Hupf, B. A. Chalmers, F. R. Knight, M. Bühl, S. Mebs, L. Chęcińska, E. Lork, P. S. Camacho, S. E. Ashbrook, K. S. Athukorala Arachchige, D. B. Cordes, A. M. Z. Slawin, J. Beckmann and J. D. Woollins, *Inorg. Chem.*, 2015, **54**, 2435–2446; (*b*) T. G. Do, E. Hupf, A. Nordheider, E. Lork, A. M. Z. Slawin, S. G. Makarov, S. Yu. Ketkov, S. Mebs, J. D. Woollins and J. Beckmann, *Organometallics*, 2015, **4**, 5341–5360.

23 K. T. Mahmudov, A. V. Gurbanov, V. A. Aliyeva, M. F. C. Guedes da Silva, G. Resnati and A. J. L. Pombeiro, *Coord. Chem. Rev.*, 2022, **464**, 214556.

24 (*a*) H. Zhao and F. P. Gabbai, *Nat. Chem.*, 2010, **2**, 984–990; (*b*) J. Y. C. Lim, I. Marques, A. L. Thompson, K. E. Christensen, V. Felix and P. D. Beer, *J. Am. Chem. Soc.*, 2017, **139**, 3122–3133.

25 A. Dessì, P. Peluso, R. Dallocchio, R. Weiss, G. Andreotti, M. Allocca, E. Aubert, P. Pale, V. Mamane and S. Cossu, *Molecules*, 2020, **25**, 2213.

26 (*a*) P. Peluso, V. Mamane, A. Dessì, R. Dallocchio, E. Aubert, C. Gatti, D. Mangelings and S. Cossu, *J. Chromatogr. A*, 2020, **1616**, 460788; (*b*) P. Peluso, C. Gatti, A. Dessì, R. Dallocchio, R. Weiss, E. Aubert, P. Pale, S. Cossu and V. Mamane, *J. Chromatogr. A*, 2018, **1567**, 119–129; (*c*) R. Dallocchio, A. Dessì, M. Solinas, A. Arras, S. Cossu, E. Aubert, V. Mamane and P. Peluso, *J. Chromatogr. A*, 2018, **1563**, 71–81; (*d*) P. Peluso, V. Mamane, R. Dallocchio, A. Dessì, R. Villano, D. Sanna, E. Aubert, P. Pale and S. Cossu, *J. Sep. Sci.*, 2018, **41**, 1247–1256; (*e*) P. Peluso, V. Mamane, E. Aubert, A. Dessì, R. Dallocchio, A. Dore, P. Pale and S. Cossu, *J. Chromatogr. A*, 2016, **1467**, 228–238.

27 (*a*) R. Weiss, E. Aubert, P. Peluso, S. Cossu, P. Pale and V. Mamane, *Molecules*, 2019, **24**, 4484; (*b*) V. Mamane, P. Peluso, E. Aubert, R. Weiss, E. Wenger, S. Cossu and P. Pale, *Organometallics*, 2020, **39**, 3936–3950; (*c*) R. Weiss, T. Golisano, P. Pale and V. Mamane, *Adv. Synth. Catal.*, 2021, **363**, 4779–4788; (*d*) E. Aubert, A. Doudouh, E. Wenger, B. Sechi, P. Peluso, P. Pale and V. Mamane, *Eur. J. Inorg. Chem.*, 2022, **2022**, e202100927; (*e*) L. Groslambert, A. Padilla-Hernandez, R. Weiss, P. Pale and V. Mamane, *Chem.–Eur. J.*, 2023, **29**, e202203372.

28 (*a*) For a general review on the importance of through-space spin-spin coupling in NCI, see: J.-C. Hierso, *Chem. Rev.*, 2014, **114**, 4838–4867; (*b*) For a recent study using ^{19}F NMR to probe the XB through the determination of through-bond $^{1}J_{C-F}$ couplings, see: B. Jimmink, D. Sethio, L. Turunen, D. von der Heiden and M. Erdélyi, *J. Am. Chem. Soc.*, 2021, **143**, 10695–10699.

29 (*a*) H. B. Singh, N. Sudha, A. A. West and T. A. Hamor, *J. Chem. Soc., Dalton Trans.*, 1990, 907–913; (*b*) For an overview, see: H. B. Singh and G. Mugesh, *Acc. Chem. Res.*, 2002, **35**, 226–236.

30 R. Weiss, Y. Cornaton, H. Khartabil, L. Groslambert, E. Hénon, P. Pale, J.-P. Djukic and V. Mamane, *ChemPlusChem*, 2022, **87**, e202100518.

31 S. Saba, J. Rafique and A. L. Braga, *Adv. Synth. Catal.*, 2015, **357**, 1446–1452.

32 A. Ouchi, T. Hyugano and C. Liu, *Org. Lett.*, 2011, **11**, 4870–4873.

33 A. Panda and H. B. Singh, *NMR of Organoselenium and Organotellurium Compounds, PATAI'S Chemistry of Functional Groups*, John Wiley & Sons, Ltd, 2013.

34 A. Hammerl, T. M. Klapötke, B. Krumm and M. Scherr, *Z. Anorg. Allg. Chem.*, 2007, **633**, 1618–1626.

35 (*a*) F. B. Mallory, E. D. Luzik Jr, C. W. Mallory and P. J. Carroll, *J. Org. Chem.*, 1992, **57**, 366–370; (*b*) F. B. Mallory, C. W. Mallory, K. E. Butler, M. B. Lewis, A. Q. Xia, E. D. Luzik Jr, L. E. Fredenburgh, M. M. Ramanjulu, Q. N. Van, M. M. Francl, D. A. Freed, C. C. Wray, C. Hann, M. Nerz-Stormes, P. J. Carroll and L. E. Chirlian, *J. Am. Chem. Soc.*, 2000, **122**, 4108–4116.

36 S. Grzesiek, F. Cordier, V. Jaravine and M. Barfield, *Prog. Nucl. Magn. Reson.*, 2004, **45**, 275–300.

37 L. Ernst and K. Ibrom, *Angew. Chem., Int. Ed.*, 1995, **34**, 1881–1882.

38 For comparison, see the $^{n}J_{C-F}$ coupling in trifluorotoluene (Hz): $^{1}J_{C-F} = 272$; $^{2}J_{C-F} = 32$; $^{3}J_{C-F} = 4$; $^{4}J_{C-F} = 1$; $^{5}J_{C-F} = 0$.

39 C. Otake, T. Namba, H. Tabata, K. Makino, K. Hirano, T. Oshitari, H. Natsugari, T. Kusumi and H. Takahashi, *J. Org. Chem.*, 2021, **86**, 4638–4645.

40 R. Ramalakshmi, K. Saha, D. K. Roy, B. Varghese, A. K. Phukan and S. Ghosh, *Chem.–Eur. J.*, 2015, **21**, 17191–17195.

41 The chemical shift for **10-Li** ($\delta_{Te} = 105.8$ ppm) is in the same range as for the known PhTeLi ($\delta_{Te} = 133.9$ ppm), see: M. A. Banks, O. T. Beachley, H. J. Gysling and H. R. Luss, *Organometallics*, 1990, **9**, 1979–1982.

42 R. Gleiter, G. Haberhauer, D. B. Werz, F. Rominger and C. Bleiholder, *Chem. Rev.*, 2018, **118**, 2010–2041.